Silicon (2021) 13:3461–3472
https://doi.org/10.1007/s12633-020-00786-7

ORIGINAL PAPER

Synthesis of Cost-Effective Hierarchical MFI-Type Mesoporous Zeolite: Introducing Diatomite as Silica Source

Morteza Servatan[1] · Mohammad Ghadiri[1] · Mohsen Khodadadi Yazdi[2] · Maryam Jouyandeh[2] · Ghader Mahmodi[3] · Ali Samadi[4] · Payam Zarrintaj[3] · Sajjad Habibzadeh[5,6] · Mohammad Reza Ganjali[2,7] · Mohammad Reza Saeb[2]

Received: 25 January 2020 / Revised: 13 October 2020 / Accepted: 14 October 2020 / Published online: 22 October 2020

Abstract

Zeolite, as an intricate microporous material with redox sites, has been widely examined in many chemical industries. However, zeolite is not available everywhere, and it is expensive considering the price of raw materials from which it can be synthesized. In this study, ZSM-5 zeolite, as a local silica source with the high crystallinity, was synthesized, based on diatomite exploited from a mine in the north-west of Iran. The diatomite was employed as the only source of silica, and underwent hydrothermal transformation in a Teflon-lined autoclave operating at 170 °C without any alkaline post-treatment. The effects of the reaction pH and the reaction time on the properties of the synthesized MFI-type zeolite were monitored. The hydrothermal reaction time was optimized and hierarchical ZSM-5 hexagonal crystals were obtained. Furthermore, the effect of Si/Al ratio on the crystallinity of the resulting zeolite was investigated. The XRD, SEM, TEM, BET, FTIR, TPD, TGA, and DSC analyses were carried out to characterize the synthesized zeolites. The results confirmed the creation of MFI-type zeolites from diatomite applying hydrothermal process at an optimized pH and reaction time. In addition, the synthesized ZSM-5 zeolites exhibited a narrow pore size distribution resembling the mesoporous structure of standard ZSM-5 zeolites. Plenty of regularly arranged pores with diameters of 300–500 nm were observed inside the round circle-like sections of diatomite. For zeolites in which Si/Al ratio was higher (55 compared to 37), a relatively narrower pore size distribution similar to that of the standard ZSM-5 zeolite was detected. Comparably, the synthesized zeolites also contained stronger acid sites, rendering it as an excellent catalyst for the conversion of methanol to gasoline.

Keywords ZSM-5 zeolite · Diatomite · Hydrothermal process · Mesoporous structure

✉ Mohammad Ghadiri
m.ghadiri@uut.ac.ir

✉ Payam Zarrintaj
payam.zarrintaj@gmail.com

[1] Department of Chemical Engineering, Urmia University of Technology, P.O. Box 57155-419, Urmia, Iran

[2] Center of Excellence in Electrochemistry, School of Chemistry, College of Science, University of Tehran, Tehran, Iran

[3] School of Chemical Engineering, Oklahoma State University, 420 Engineering North, Stillwater, OK 74078, USA

[4] Department of Polymer Engineering, Faculty of Engineering, Urmia University, Urmia, Iran

[5] Department of Petrochemical Engineering, Amirkabir University of Technology, Tehran, Iran

[6] Department of Chemical Engineering, Amirkabir University of Technology, Tehran, Iran

[7] Biosensor Research Center, Endocrinology and Metabolism Molecular-Cellular Sciences Institute, Tehran University of Medical Sciences, Tehran, Iran

1 Introduction

Porous-silica-based materials are widely employed in various applications including controlled drug delivery, catalysis, thermal insulators, and bio molecular separation [1–3]. In particular, functionalized mesoporous silica-based products, e.g., zeolites, which encompass organic and inorganic groups together within their mesoporous structures, are promising candidates for newly-emerged heterogeneous catalysts, adsorbents, and ion-exchangers [4, 5]. However, relatively small pore size of microporous zeolites may mitigate the diffusion rate of reactants and products into and from the active sites inside the zeolite crystals. Such phenomenon limits the industrial application of zeolites [6–10].

Hierarchical zeolites are commonly prepared through a post-treatment or secondary template synthesis method [11, 12]. Notwithstanding, a large number of secondary templates including carbons [13–15], amines [16, 17], cationic polymers [18, 19], polyvinyl butyral gels [20, 21], amphiphilic organosilanes

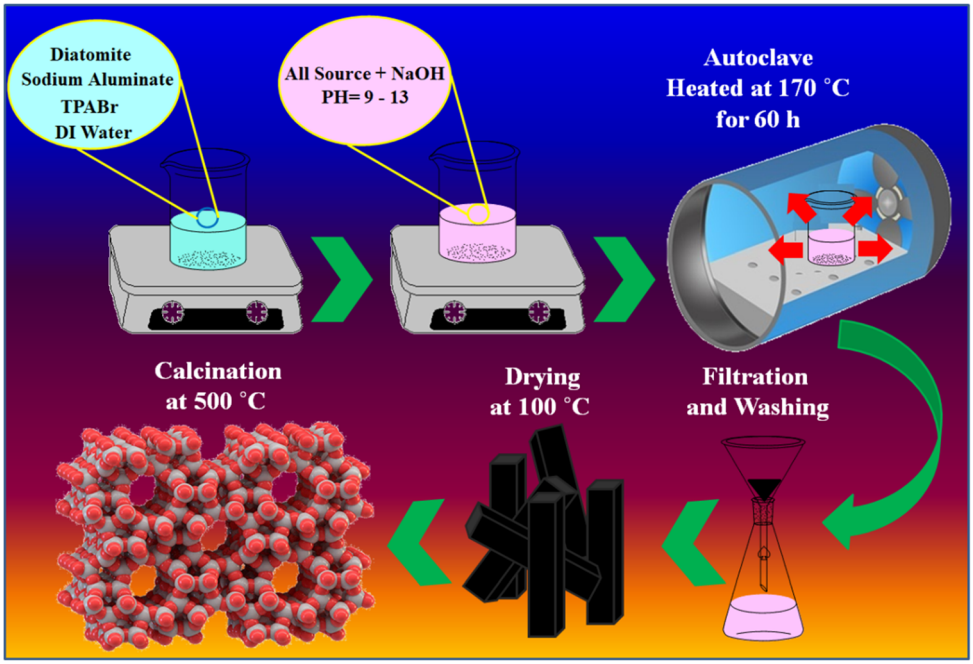

Fig. 1 Schematic of the preparation steps of nanostructured HZSM-5

[22, 23], soluble starch or sodium carboxy methylcellulose [24–26] have been used in the hierarchical zeolites. However, industrial applications of these hierarchical zeolites are still limited because of the complexity of synthesis processes and high costs of the raw materials. MFI-type zeolites, e.g., ZSM-5, have been regarded as the potential adsorbents and catalysts due to their high strong acid sites, favored micro channels, large surface area, and acceptable thermal stability [27–29].

Zeolites are primarily synthesized from sodium aluminosilicate sources, which form gels containing different commercial silica and alumina reagents [30, 31]. However, ever-increasing consumption of zeolites in recent years resulted in employing the commercial silica and alumina sources; hence, elevated the product cost. Therefore, cheaper raw materials are required to reduce the cost of the synthesized zeolites. Since natural aluminosilicate minerals possess the desired characteristics, several attempts have been made to synthesize ZSM-5 from kaolin [32], rectorite [33], palygorskite [34] and attapulgite [35]. Although the low SiO_2/Al_2O_3 ratio of the natural aluminosilicate minerals might not meet that of ZSM-5, an appropriate modification can effectively tackle such a problem.

Diatomite is fine-grained, low density biogenic sediment, comprising amorphous hydrated silica ($SiO_2.nH_2O$) derived from opalescent frustules of diatoms [36]. Diatoms are a class of microalga with hard and porous cell walls mainly composed of silica, but showing different morphologies and micro/nano pores [37, 38]. Diatomite has been previously used to synthesize diatomite/zeolite composites benefiting from its silica-based macroporous structure, which improved the efficiency of mass transfer process (i.e. diffusion). Yu et al. [36] prepared a diatomite/ZSM-5 composite through the hydrothermal treatment of an ultrasonic seeded diatomite in a solution containing a silica source. They reported a high water diffusion rate. Wang et al. used a vapor-phase transport (VPT) method in order to prepare diatomite/MFI-type zeolite composites [39].

Table 1 Elemental analysis of diatomite before and after acid leaching and the final composition of the synthesized zsm-5 Zeolite

diatomite before acid leaching		diatomite after acid leaching		zsm-5 Zeolite	
Formula	(%)	Formula	(%)	Formula	(%)
SiO_2	91.85	SiO_2	94.25	SiO_2	97.2
Al_2O_3	1.42	Al_2O_3	1.21	Al_2O_3	2.142
Fe_2O_3	0.48	Fe_2O_3	0.21	Fe_2O_3	0.11
CaO	0.52	CaO	0.17	CaO	0.10
MgO	0.36	MgO	0.23	MgO	0.12
Na_2O	0.26	Na_2O	0.11	Na_2O	0.24
L.O.I	4.98	L.O.I	3.8	L.O.I	–

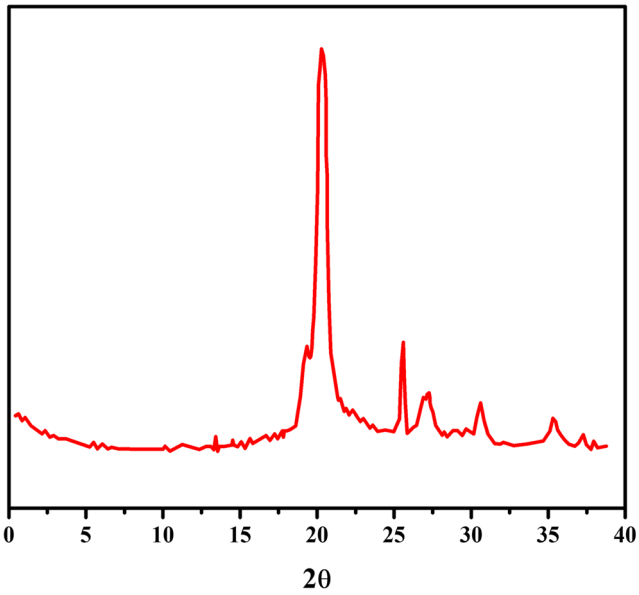

Fig. 2 X-ray diffraction patterns for Diatomite after purification

However, optimization of microstructure of such silica materials has not been fully addressed.

This study aims to facilitate the large scale production of ZSM-5 through the cost-effective silica-based material, diatomite that has been exploited from a mine in north-west of Iran. To address this objective, the effect of different parameters such as reaction time (24, 48 and 60 h) and Si/Al ratios (37 and 55) on the properties of the synthesized zeolite were studied. The X-ray diffraction (XRD), scanning electron microscopy (SEM), transmissive electron microscopy (TEM), Brunauer-Emmett-Teller (BET), Fourier-transform infrared spectroscopy (FTIR), Temperature programmed desorption (TPD), thermogravimetric analysis (TGA), and differential scanning calorimetry (DSC) analyses were performed for the characterization of the synthesized zeolites.

2 Experimental

2.1 Chemicals and Materials

Sodium aluminate as the alumina source, Tetra propyl ammonium bromide (TPABR), the template, sulfuric acid and sodium hydroxide were purchased from Merck Chemical Company. Diatomite as the silica source (containing 91.4 wt.% SiO_2, 3.5 wt.% Al_2O_3 and 2.2 wt.% Fe_2O_3) was purchased from west Azerbaijan mines in the north-west of Iran.

2.2 ZSM-5 Synthesis

The natural diatomite was treated through a thermal activation method at 500 °C for 2 h. Then, Fe_2O_3 and organic chemicals were washed out via an aqueous solution of 2 M H_2SO_4 at 100 °C for 4 h while stirring under reflux and controlled temperature. Next, the mixture was filtered, washed thoroughly with deionized water and dried at 100 °C.

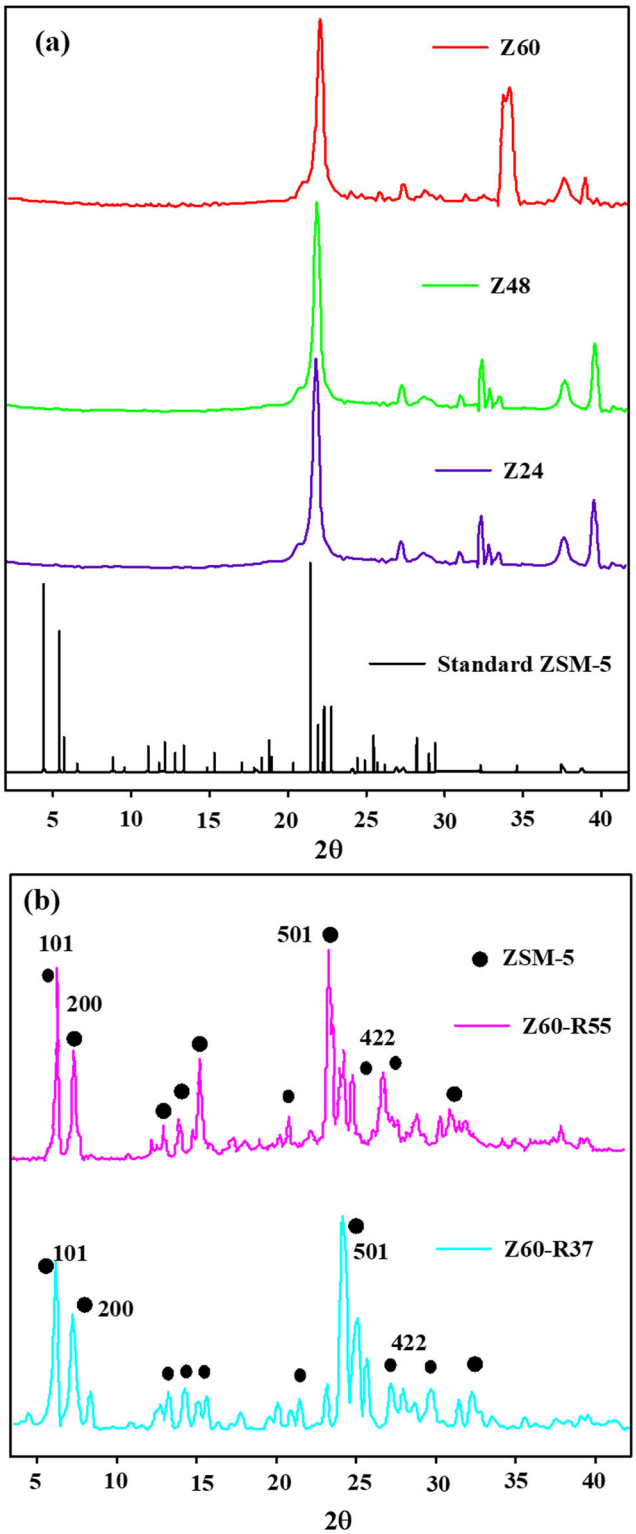

Fig. 3 X-ray diffraction patterns for **a**) standard ZSM-5 and zeolite with different reaction time and **b**) different Si/Al ratio after hydrothermal reaction

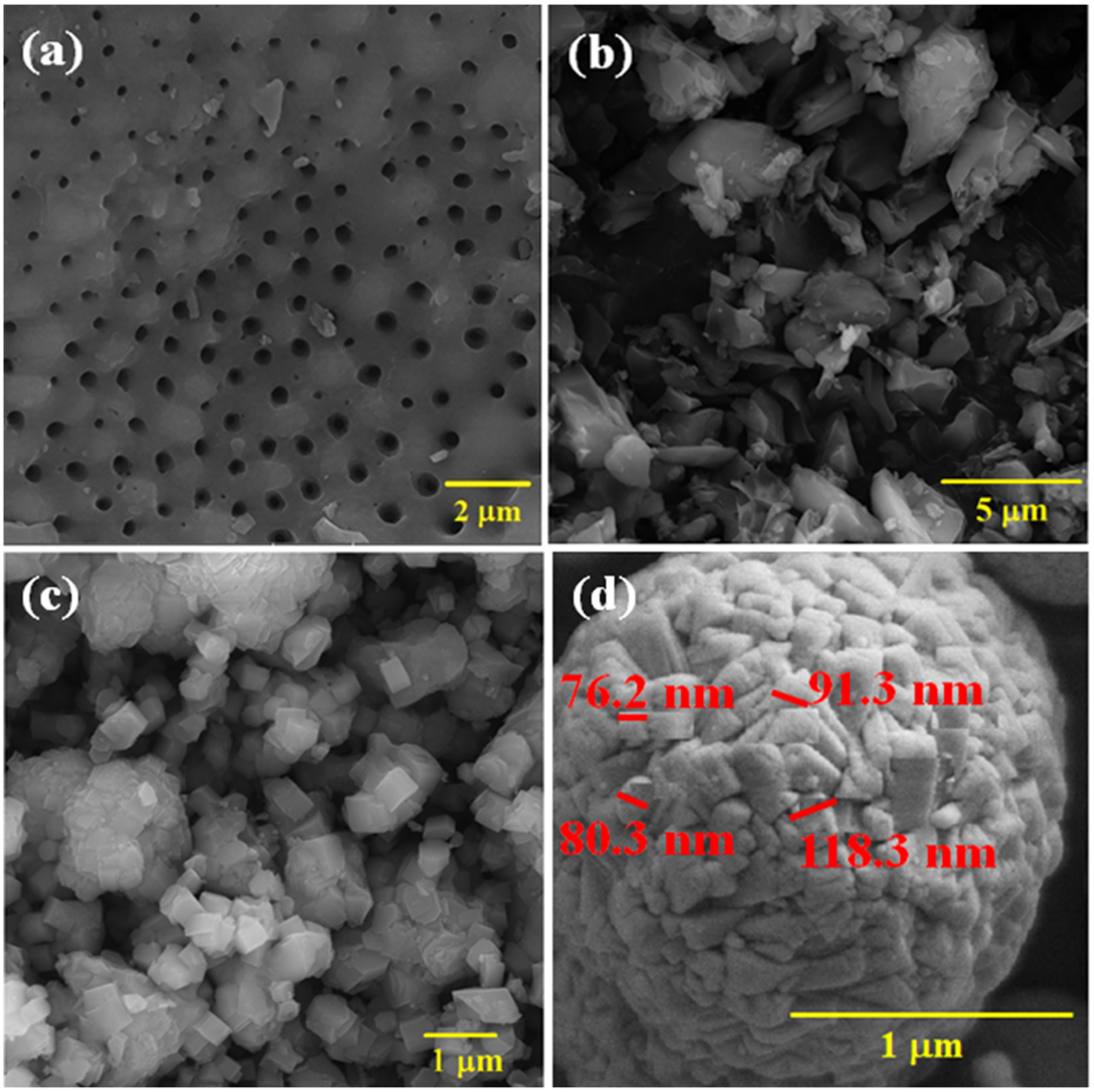

Fig. 4 SEM images of **a**) diatomite, **b**, **c**) ZSM-5 zeolite with Si/Al ratio of 37 and 55 respectively, and **d**) spherical aggregates

The synthesis procedure of HZSM-5 via the hydrothermal method [40] passed through the steps depicted in Fig. 1.

Namely, 2.21 g of purified diatomite, 0.24 g sodium aluminate, 1.6 g TPABr and certain amount of deionized water were mixed. The final pH of the mixture was adjusted to 10 by dropwise addition of sodium hydroxide under vigorous stirring for 1 h at room temperature. The resulting mixture was transferred into a Teflon-lined stainless steel autoclave in which the hydrothermal process was carried out at 170 °C for 60 h under the autogenous pressure. The precipitate was filtered, washed thoroughly with deionized water for several times and dried at 100 °C for 24 h which is followed by calcination at 500 °C for 6 h to form Na-ZSM-5. The as-synthesized powder was obtained without the organic template. Lastly, the obtained Na-ZSM-5 was treated by ion exchange agent (NH_4NO_3) for 6 h at 80 °C, filtered, washed with distilled water and air dried. The HZSM-5 form was obtained finally via calcination at 500 °C for 4 h. The elemental analysis of diatomite before and after acid leaching and the final composition of the synthesized zsm-5 Zeolite are provided in Table 1.

2.3 Characterizations

The crystallinity of the prepared samples was characterized by X-ray diffraction (XRD) using Siemens diffractometer D5000 in the range of $2\theta = 0–45$ with mono-chromatized Cu-kα radiation with an X-ray tube operated at 30 mA and 40 kV. Diffraction patterns were identified by comparing with those included in the Joint Committee of Powder Diffraction Standards (JCPDS) data base. Crystal sizes of HZSM-5 were estimated using the Scherrer equation. Fourier transform infrared (FTIR) spectroscopy analysis was used as a complementary tool to the XRD to characterize the structure of zeolite. The spectral data were recorded by Unicam 4000

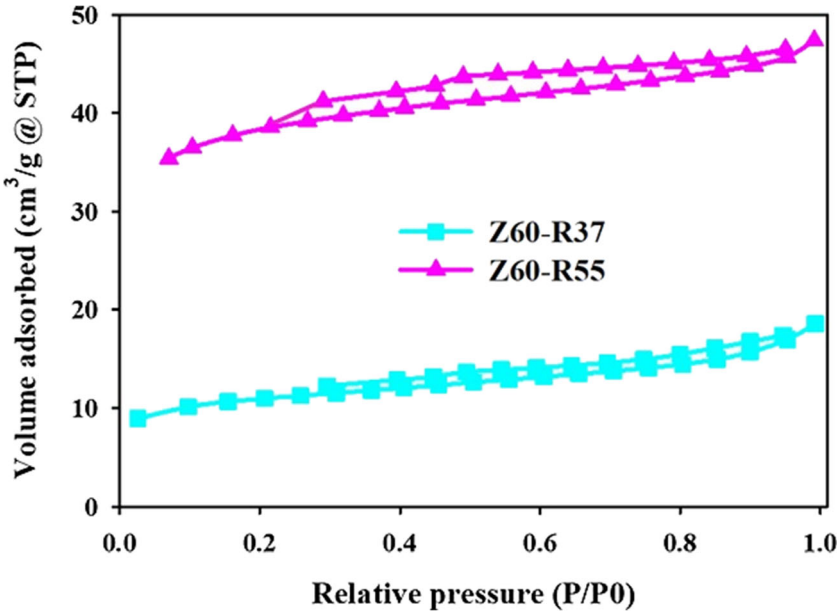

Fig. 5 The BET nitrogen sorption–desorption isotherms

FTIR spectrometer using KBr, collecting spectra in the range of 400–4000 cm^{-1}. The morphology and microstructure of samples were observed by field emission scanning electron microscope (FESEM) HITACHI S-4160. The specific surface area of the synthesized samples were measured by nitrogen adsorption-desorption isotherms at -196 °C using Quantachrom Chem BET-3000 apparatus; the samples were degassed at 300 °C prior to the measurement .

Temperature programmed desorption of ammonia (NH_3-TPD) was carried out with a thermal conductivity detector. Certain amount of the samples was placed in a quartz tubular reactor and pretreated at 900 °C in an argon stream. After cooling to 100 °C, gaseous NH_3 was passed through the sample for 30 min. Finally, the NH_3-TPD curve of the sample was recorded by programmed heating from 100 to 900 °C with a heating rate of 10 °C/min after removal of physically adsorbed NH_3 by flowing argon for 2 h at 100 °C.

3 Results and Discussions

The XRD pattern of Diatomite after purification is shown in Fig. 2. As it can be seen there is some Quartz content present in Diatomite sample and 2θ peaks of 19.3, 30.7 and 36 can be assigned to this material. However, after hydrothermal reaction, according to Fig. 3, these patterns were not present in Zeolites XRD diffractograms, which proves successful conversion of raw Diatomite to an Aluminosilicate framework.

Figure 3a shows the XRD patterns of standard ZSM-5, as well as zeolite synthesized applying 24, 48 and 60 h reaction time, which are denoted as standard Z24, Z48 and Z60, respectively. In addition, the samples of Z60 synthesized with Si/Al ratios of 37 and 55, which are represented by Z60-R37 and Z60-R55, respectively (Fig. 3b). A comparison between the synthesized diffractograms and the standard pattern confirms the presence of ZSM-5 in the tetragonal phase. Furthermore, it can be seen that the crystalline growth increases as the hydrothermal process time proceeds. Namely, the structure seems to be crystalline phase in the form of cristobalite for the reaction time is less than 60 h [41]. However, the weak peaks at 2 of 7.8, 8.8, 22.9, 23.7, and 24.5, can be assigned to MFI topology detected in the sample Z60-R37. Typical diffraction lines corresponding to the ZSM-5 are observed for samples Z60-R37 and Z60-R55, indicating that changing the silica source from the typical organic materials to a natural inorganic material, i.e., diatomite, has no obvious influence on the crystalline structure of the synthesized ZSM-5. XRD patterns further confirmed the high purity and crystallinity of the obtained zeolite [42].

The SEM images of diatomite and as-synthesized samples are compared in Fig. 4. As it can be seen, diatomites are mostly disc-like structures adjunct to each other with diameters around 100 nm (Fig. 4). Moreover, plenty of regularly arranged pores with diameters of 300–500 nm were observed inside the round circle-like sections of diatomite (Fig. 4a). However, the starting diatomite considerably transformed into ZSM-5 (Z60-R37) during hydrothermal process (Fig. 3b and Fig. 4b). Furthermore, at higher Si/Al ratios (Fig. 4c), we can notice that uniformly-sized cubic structure with a unit size of 0.6 μm are formed. However, some of the cubes formed with smaller sizes are mingled with the larger ones, resulting in pseudo-spherical aggregates and layers of thin films together with

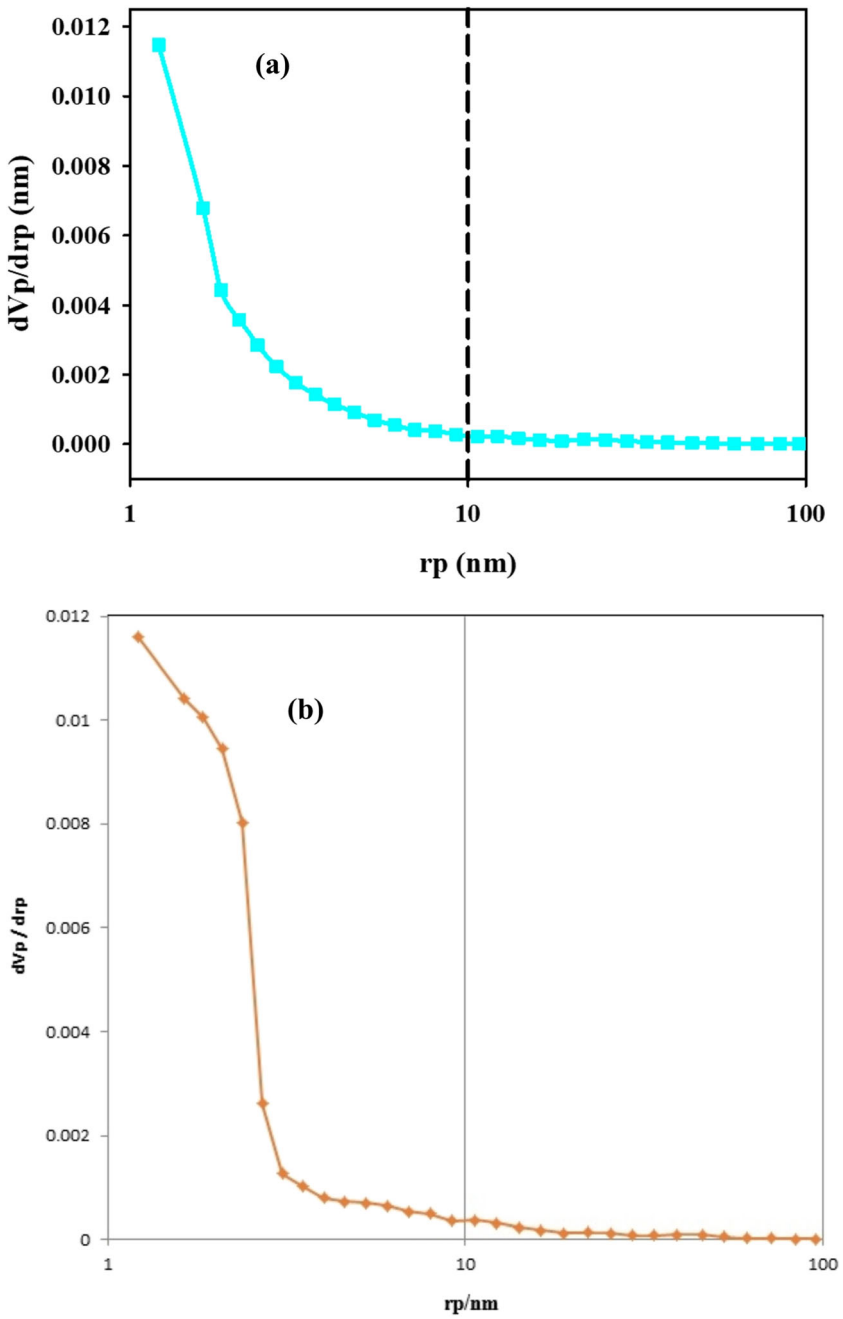

Fig. 6 The BJH plot for (**a**) Z60-R55 and (**b**) Z60-R37

egg-like particles (Oswald ripening). Particle size of such spherical aggregates range is from 70 to 120 nm (Fig. 4d).

The N_2 adsorption–desorption isotherms of the synthesized samples are presented in Fig. 5. The hysteresis loops in the adsorption-desorption isotherms at various relative pressure (P/P_0 from 0.35 to 1.0) may be attributed to the mesoporous structures of Z60-R37 and Z60-R55. Both the hysteresis loops behave as type I isotherm. Furthermore, the wider hysteresis loop for the case of Z60-R55 compared to the Z60-R37 can be ascribed to the gases adsorbed; considering that the former adsorbed more gas (four times more), suggesting a microporous structure.

Figure 6 shows the pore size distribution of Z60-R55 sample, which is estimated using BJH method. The results of the pore size distribution show that the sample has a relatively narrow pore-size distribution with mesopores having size in the range of 2–10 nm. This outcome is similar to the pore size of the standard ZSM-5 zeolite [43].

The textural properties of the zeolites and raw diatomite are compared in Table 2. BET surface area, micro and mesopore volumes and the total pore volume of Z60-R55 zeolite are obviously much higher than those reported for the diatomite used in this study. The values of Z60-R37 are located between

Table 2 Textural properties of the zeolites and raw diatomite

Sample	Si/Al	Surface Area (m^2g^{-1})	Pore Volume (micro) (cm^3g^{-1})	Pore Volume (meso) (cm^3g^{-1})	Pore Volume (Total) (cm^3g^{-1})	Crystal Size	Pore Diameter (nm)
Diatomite	64	2.00					
Z60-R37	37	97.08	0.1284	0.1569	0.28535	74	2.89
Z60-R55	55	154.36	0.2170	0.5143	0.73136	51	2.05

the raw diatomite and Z60-R55, but the numbers reported are mostly close to the other ZSM-5 sample. Therefore, there is a meaningful gap compared to the diatomite, implying that hydrothermal process successfully converted the amorphous diatomite to ZSM-5 nanostructures. As shown in Table 2, the total pore volume for Z60-R55 is significantly larger than those for Z60-R37. This can be correlated with textural features of Z60-R55. For Z60-R37, it possessed much low surface area, which may be due to the collapse of zeolite nanosheets [44].

Figure 7 shows the FTIR spectra of the samples synthesized by the hydrothermal method. As it can be noticed, the IR spectra of all synthesized samples are similar with no significant differences. However, the intensity and the area of the peaks are different. Vafaeian et al. [45] indicated that the observed peaks in the interval of 450–1200 cm^{-1} are mostly related to the various zeolite types present in the samples structure. The peak at 463 cm^{-1} is assigned to TOT (where T denotes Si or Al) bending vibration. The spectrum peak at 555 cm^{-1} can be ascribed to the asymmetric stretching mode of the double five-membered rings (D5R) of the pentasil ZSM-5 zeolite structure. The peak at 3443 cm^{-1} is attributed to the bridging OH groups and interacting OH [46]. The other peak at 1632 cm^{-1} is observed due to the physically adsorbed water [47]. Moreover, the characteristic symmetric and asymmetric TOT (where T denotes Si or Al) bending vibration modes are detected at 750–850 cm^{-1} and 1100–1200 cm^{-1}, respectively. Consequently, these bands further confirm highly crystalline diatomite-based ZSM-5 zeolite synthesized in this study.

In order to investigate the structural properties of the synthesized samples in detail, transmission electron microscopy (TEM) was used. Figure 8 shows TEM images of the synthetized catalyst. It was reported that there are many factors such as “zeolite-like” connectivity, high temperature synthesis, and salt effect, which are favorable for the

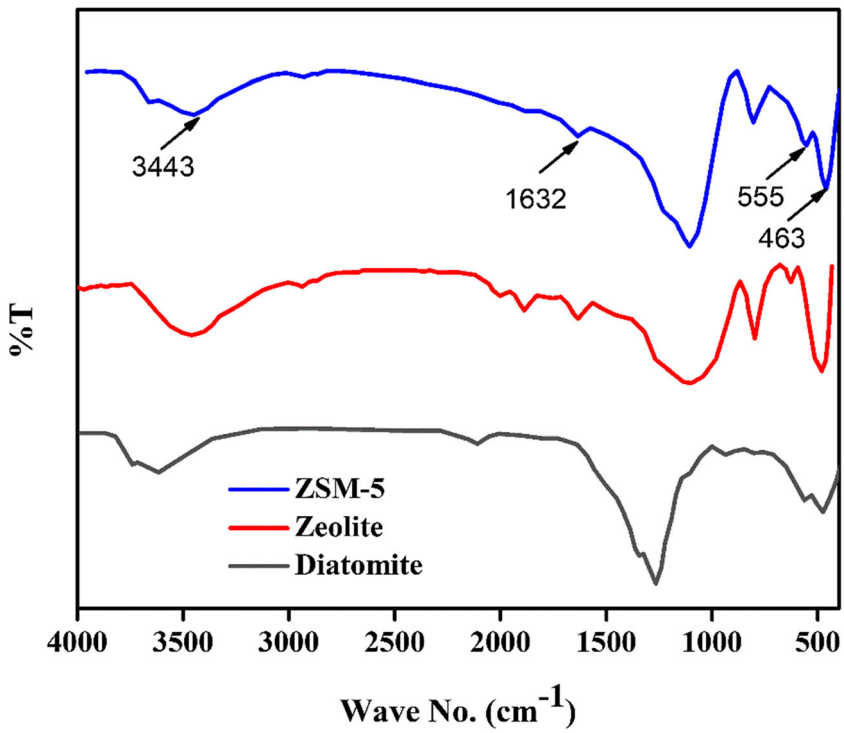

Fig. 7 FTIR spectrum of the ZSM-5 sample synthesized by conventional hydrothermal method and the spectra of zeolite and diatomite

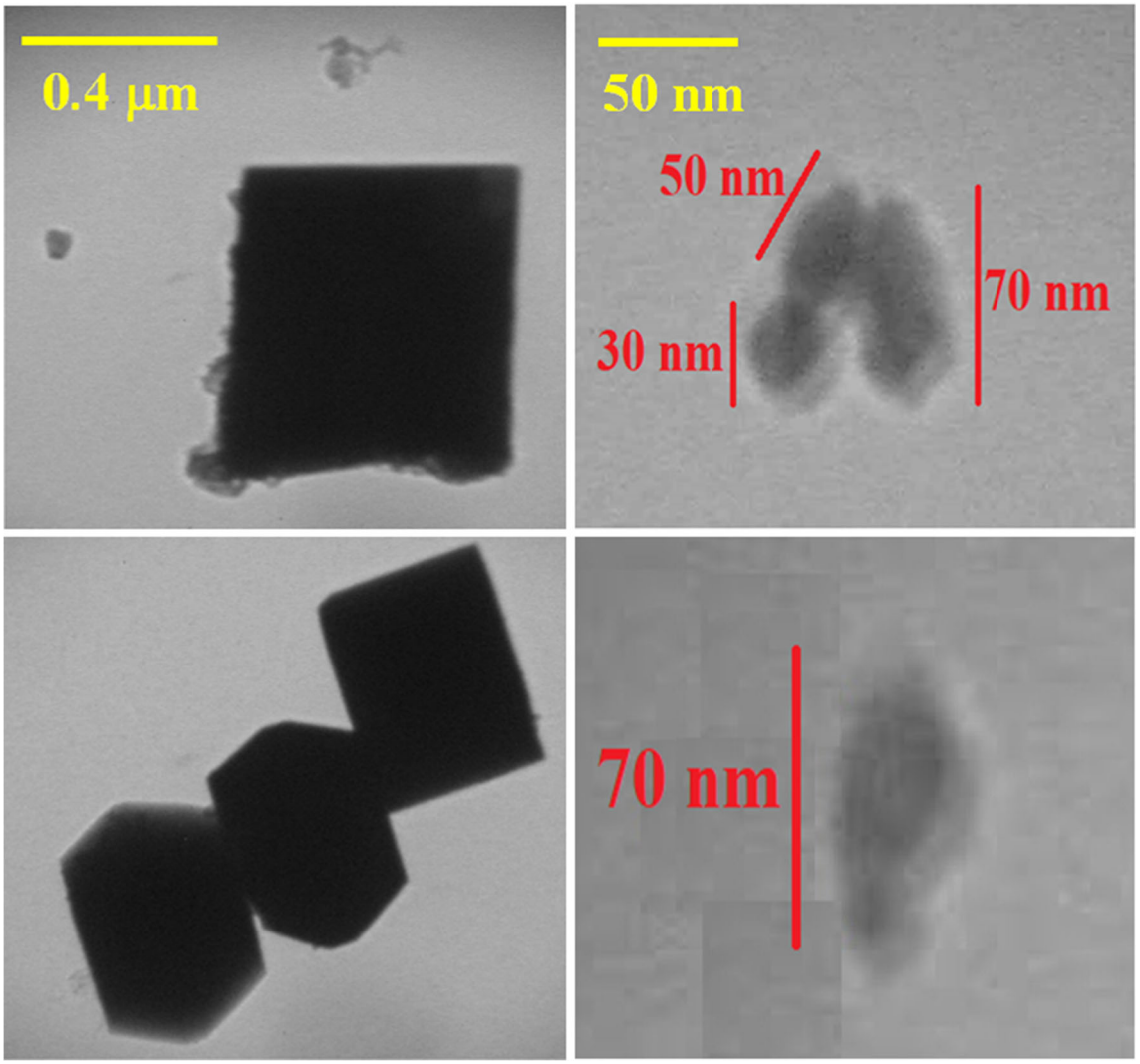

Fig. 8 TEM images of the synthesized zeolite sample

hydrothermal stability of the mesoporous materials [5, 8, 9, 20, 21]. Taking these factors into account, the remarkable special shape of ZSM-5 zeolite can be clearly observed. The core of ZSM-5 crystals can be removed by base treatment resulting in hollow zeolites with diameters below 50 nm.

The XRD patterns for the synthesized ZSM-5 zeolites at various pH are shown in Fig. 9. This analysis clearly indicates that zeolite synthesis is dependent upon the acidity of the hydrothermal starting batch. Figure 9a shows the XRD for the standard ZSM-5, while the other diffractograms illustrate the effect of pH value on the X-ray diffraction patterns of the samples. Consequently, in acidic solutions no significant peak has been recorded (Fig. 9b), means that the amorphous structure of the raw materials is not changed. However, as the pH values gradually increase up to 5 or 7, some of the zeolite phase peaks begin to rise in 2θ angles greater than 20, (ca. 22.1° and 36.2°). This suggests the rearrangement of Si-O bonds and that new zeolite structures shaping the process are partially formed. Further increase of pH up to 10 led to a promising crystalline structure of ZSM-5 zeolite (see Fig. 9).

Electrical properties of the zeolite samples stem from hydroxyl groups (i.e. Si–OH) and aluminum–oxygen tetrahedrons. ZSM-5 contains both the charge sites. The negative charges of aluminum–oxygen tetrahedrons are considered to be stronger than those of surface silicon hydroxyl groups. The silicon hydroxyl causes a negative charge in ZSM-5 zeolite structure. The XRD patterns of the prepared zeolites with different Si/Al ratio are plotted in Fig. 3. Typical diffraction peaks corresponding to the ZSM-5 zeolites are observed in both samples with similar hydrothermal seeding time. This suggested that Si/Al ratio has no obvious effect on the framework structure of ZSM-5 synthesized by hydrothermal procedure. However, the recorded intensities of the sample with higher Si/Al ratio are found to be higher than that of the ZSM-5 zeolite with lower Si/Al ratio, demonstrating the

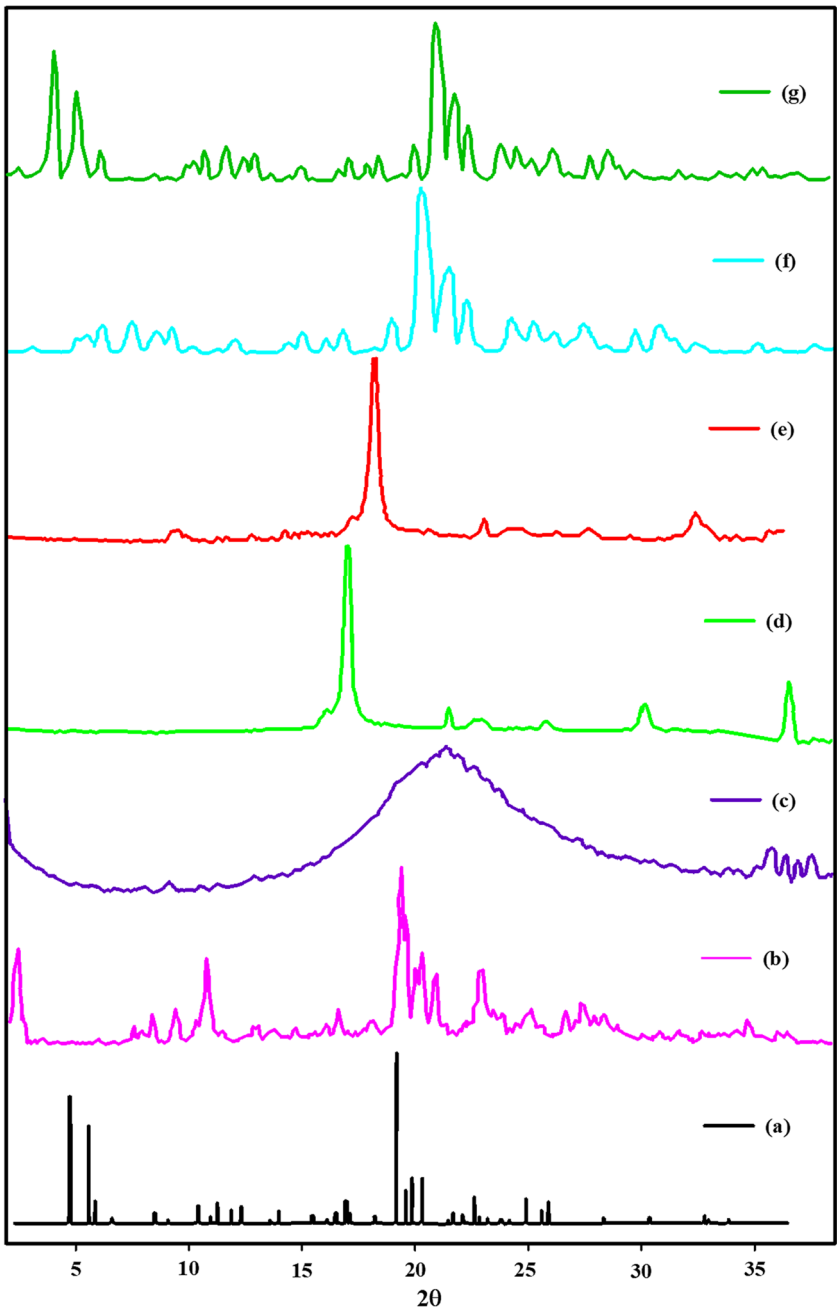

Fig. 9 X-ray diffraction of catalysts synthesized at different pH values. **a** Standard, **b** Z60-R37, **c** pH = 4, **d** pH = 5, **e** pH = 7, **f** pH = 10, **g** PH = 12

higher crystallinity due to lower Al incorporation. Moreover, X-ray absorption coefficient decreases with increasing the Si/Al ratio, because of low Al content, leading to the sharper peaks in XRD pattern of zeolite Z60-R55.

TPD analysis was performed to evaluate the strength of the acidic sites and desorbed species on the surface by increasing the temperature [48]. NH_3-TPD profile for ZSM-5 zeolite (Z60-R55 and Z60-R37) is depicted in Fig. 10. The TPD plot of catalyst shows temperature peaks at about 140 and 405 °C in Z60–37, while at 180 and 420 °C in Z60-R37 sample. The peaks at 140 and 180 °C can be attributed to the weak acidic sites, while those at 405 and 420 °C can be attributed to the strong acid sites. It would then be expected that the zeolites with higher Si/Fe ratios show higher-temperature ammonia desorption. The peaks at relatively low temperatures, i.e. 140–330 °C represent the chemisorbed NH_3 on non-acidic/weak acid sites [49]. On the other hand, normal desorption peaks observed at 375 °C or higher temperatures can be attributed to the desorption of ammonia from strong acid sites [50]. This result proves that there are both strong acid sites along with weak and medium acid sites present in the synthesized zeolites. The changes in the acidic properties

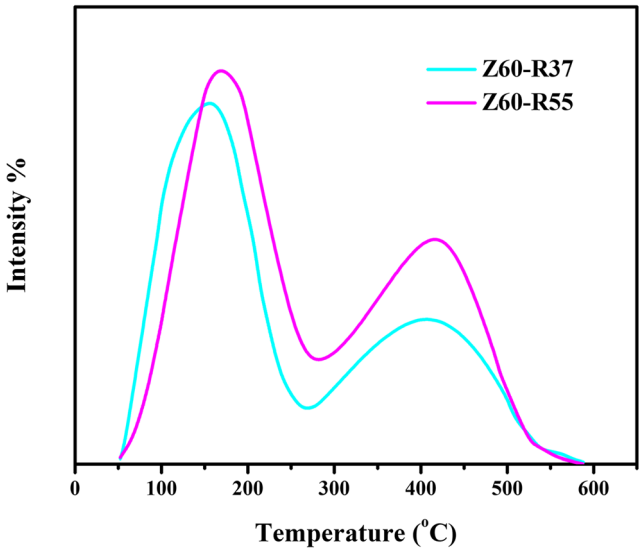

Fig. 10 Temperature programmed desorption (TPD) spectrum of ZSM-5 zeolite (Z60-R55 and Z60–37)

resulting from surface characteristics may alter catalytic performance of the nanocrystalline zeolites used in catalytic processes.

The results of the DSC and TGA analyses conducted on ZSM-5 zeolite are illustrated in Fig. 11. The TGA and DSC profiles of Z60-R55 show two major weight losses in 50–250 °C and 250–650 °C range. The first significant weight loss, approximately 6.70%, is due to the water desorption from zeolite pore walls. The second weight reduction of 10% is most likely attributed to the decomposition of an organic compound, such as remaining directing agent molecules in the zeolite structure. The decomposition at around 300–450 °C could be explained by the removal of cations from the micro pores [51]. It is also observed that the structure of the synthesized H-ZSM-5 zeolite remain unchanged up to about 650 °C. The sharp reduction that occurs beyond 650 °C is mainly due to the collapsing zeolite structures to an amorphous phase followed by recrystallization to non-zeolitic materials.

4 Conclusion

In this study, the hydrothermal process was used in order to synthesis of zeolite-based catalysts from diatomite minerals without alkaline post treatment. Moreover, the effects of different parameters including time duration of hydrothermal process and the pH of the hydrothermal environment on the synthesized zeolite are investigated using different techniques. The reaction time was optimized to form hierarchical ZSM-5 hexagonal crystals. Comparing the SEM images before and after hydrothermal process it was understood that disc-like structures of diatomite diminished, while zeolite nanoparticles emerged gradually. Furthermore, SEM and BET results showed that for zeolites with higher Si/Al ratio (55 compared to that of 37) a relatively narrower pore size distribution (similar to standard ZSM-5 zeolites) was likely to happen. In fact, decreasing Al in the zeolite structure resulted in more crystallinity, as proved by XRD analysis. Moreover, a more mesoporous structure was observed for Z60-R55 similar to the standard ZSM-5 zeolites. The synthesized zeolites showed high thermal stability and also possessed many strong acid sites along with some weak/medium acid sites. These results suggest that diatomite minerals can be considered as abundant inexpensive raw materials for manufacturing MFI-type catalyst zeolites, to be used as catalyst in conversion of methanol to gasoline.

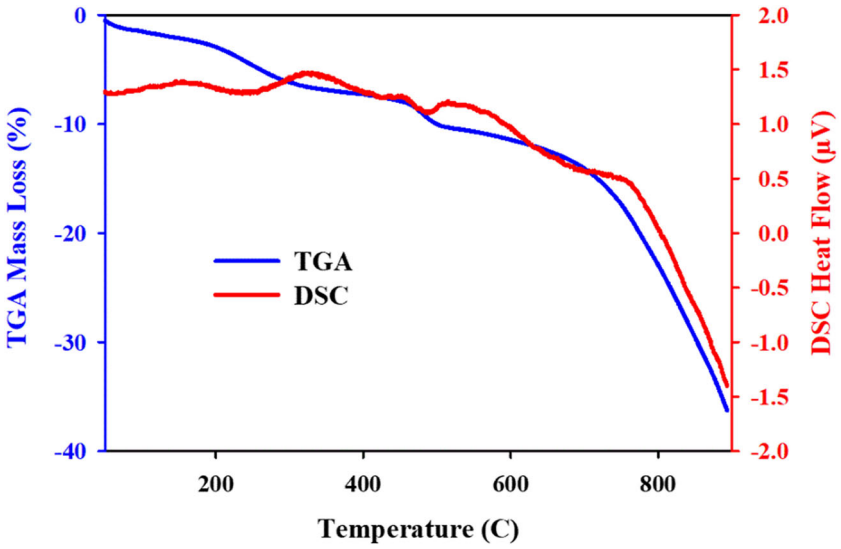

Fig. 11 TGA/DSC diagrams for ZSM-5 zeolite

References

1. Rimer JD (2018) Rational design of zeolite catalysts. Nat Catalysis 1(7):488
2. Ghiyasi S, Sari MG, Shabanian M, Hajibeygi M, Zarrintaj P, Rallini M, Torre L, Puglia D, Vahabi H, Jouyandeh M (2018) Hyperbranched poly (ethyleneimine) physically attached to silica nanoparticles to facilitate curing of epoxy nanocomposite coatings. Prog Org Coat 120:100–109
3. Mahmodi G, Dangwal S, Zarrintaj P, Zhu M, Mao Y, Mcllroy DN, Saeb MR, Vatanpour V, Ramsey JD, Kim S-JJS, Technology P (2020) NaA zeolite-coated meshes with tunable hydrophilicity for oil-water separation. Sep Purif Technol 240:116630
4. Přech J, Pizarro P, Serrano DP, Čejka J (2018) From 3D to 2D zeolite catalytic materials. Chem Soc Rev 47(22):8263–8306
5. Mahmodi G, Zarrintaj P, Taghizadeh A, Taghizadeh M, Manouchehri S, Dangwal S, Ronte A, Ganjali MR, Ramsey JD, Kim S-JJCR (2020) From microporous to mesoporous mineral frameworks: an alliance between zeolite and chitosan. Carbohydr Res 489:107930
6. Čejka J, Centi G, Perez-Pariente J, Roth WJ (2012) Zeolite-based materials for novel catalytic applications: opportunities, perspectives and open problems. Catal Today 179(1):2–15
7. Servatan M, Ghadiri M, Damanabi AT, Bahadori F, Zarrintaj P, Ahmadi Z, Vahabi H, Saeb MR (2018) Zeolite-based catalysts for exergy efficiency enhancement: the insights gained from nanotechnology. Mater Today: Proc 5(7):15868–15876
8. Servatan M, Zarrintaj P, Mahmodi G, Kim S-J, Ganjali MR, Saeb MR, Mozafari MJDDT (2020) Zeolites in drug delivery: Progress, challenges and opportunities. Drug Discov Today 25(4):642–656
9. Zarrintaj P, Mahmodi G, Manouchehri S, Mashhadzadeh AH, Khodadadi M, Servatan M, Ganjali MR, Azambre B, Kim SJ, Ramsey JDJM (2020) Zeolite in tissue engineering: opportunities and challenges. Curr Opin Clin Nutr Metabol Care 1(1):5–34
10. Yazdi MK, Zarrintaj P, Hosseiniamoli H, Mashhadzadeh AH, Saeb MR, Ramsey JD, Ganjali MR, Mozafari MJJMCB (2020) Zeolites for theranostic applications. J Mater Chem B 8(28):5992–6012
11. Verboekend D, Pérez-Ramírez J (2011) Design of hierarchical zeolite catalysts by desilication. Catalysis Sci Technol 1(6):879–890
12. Lopez-Orozco S, Inayat A, Schwab A, Selvam T, Schwieger W (2011) Zeolitic materials with hierarchical porous structures. Adv Mater 23(22–23):2602–2615
13. Wang B, Côté AP, Furukawa H, O'Keeffe M, Yaghi OM (2008) Colossal cages in zeolitic imidazolate frameworks as selective carbon dioxide reservoirs. Nature 453(7192):207
14. Derakhshandeh MR, Eshraghi MJ, Hadavi MM, Javaheri M, Khamseh S, Sari MG, Zarrintaj P, Saeb MR, Mozafari M (2018) Diamond-like carbon thin films prepared by pulsed-DC PE-CVD for biomedical applications. Surf Innov 6(3):167–175
15. Derakhshandeh MR, Eshraghi MJ, Javaheri M, Khamseh S, Sari MG, Zarrintaj P, Saeb MR, Mozafari M (2018) Diamond-like carbon-deposited films: a new class of biocorrosion protective coatings. Surf Innov 6(4–5):266–276
16. Chatti R, Bansiwal AK, Thote JA, Kumar V, Jadhav P, Lokhande SK, Biniwale RB, Labhsetwar NK, Rayalu SS (2009) Amine loaded zeolites for carbon dioxide capture: amine loading and adsorption studies. Microporous Mesoporous Mater 121(1–3):84–89
17. Zarrintaj P, Urbanska AM, Gholizadeh SS, Goodarzi V, Saeb MR, Mozafari M (2018) A facile route to the synthesis of anilinic electroactive colloidal hydrogels for neural tissue engineering applications. J Colloid Interface Sci 516:57–66
18. Wang L, Zhang Z, Yin C, Shan Z, Xiao F-S (2010) Hierarchical mesoporous zeolites with controllable mesoporosity templated from cationic polymers. Microporous Mesoporous Mater 131(1–3):58–67
19. Mohebbi S, Nezhad MN, Zarrintaj P, Jafari SH, Gholizadeh SS, Saeb MR, Mozafari M (2019) Chitosan in biomedical engineering: a critical review. Curr Stem Cell Res Ther 14(2):93–116
20. Zhu H, Liu Z, Kong D, Wang Y, Yuan X, Xie Z (2009) Synthesis of ZSM-5 with intracrystal or intercrystal mesopores by polyvinyl butyral templating method. J Colloid Interface Sci 331(2):432–438
21. Zhu H, Liu Z, Kong D, Wang Y, Xie Z (2008) Synthesis and catalytic performances of mesoporous zeolites templated by polyvinyl butyral gel as the mesopore directing agent. J Phys Chem C 112(44):17257–17264
22. Choi M, Cho HS, Srivastava R, Venkatesan C, Choi D-H, Ryoo R (2006) Amphiphilic organosilane-directed synthesis of crystalline zeolite with tunable mesoporosity. Nat Mater 5(9):718
23. Cheneviere Y, Chieux F, Caps V, Tuel A (2010) Synthesis and catalytic properties of TS-1 with mesoporous/microporous hierarchical structures obtained in the presence of amphiphilic organosilanes. J Catal 269(1):161–168
24. Thipmanee R, Sane A (2012) Effect of zeolite 5A on compatibility and properties of linear low-density polyethylene/thermoplastic starch blend. J Appl Polym Sci 126(S1):E252–E259
25. Yarahmadi E, Didehban K, Sari MG, Saeb MR, Shabanian M, Aryanasab F, Zarrintaj P, Paran SMR, Mozafari M, Rallini M (2018) Development and curing potential of epoxy/starch-functionalized graphene oxide nanocomposite coatings. Prog Org Coat 119:194–202
26. Sari MG, Vahabi H, Gabrion X, Laheurte P, Zarrintaj P, Formela K, Saeb MR (2018) An attempt to mechanistically explain the viscoelastic behavior of transparent epoxy/starch-modified ZnO nanocomposite coatings. Prog Org Coat 119:171–182
27. Mentzen BF (2007) Crystallographic determination of the positions of the monovalent H, Li, Na, K, Rb, and Tl cations in fully dehydrated MFI type zeolites. J Phys Chem C 111(51):18932–18941
28. Hernandez M, Rojas F, Lara V (2000) Nitrogen-sorption characterization of the microporous structure of clinoptilolite-type zeolites. J Porous Mater 7(4):443–454
29. Karbassi M, Zarrintaj P, Ghafarinazari A, Saeb M, Mohammadi MR, Yazdanpanah A, Rajadas J, Mozafari M (2018) Microemulsion-based synthesis of a visible-light-responsive Si-doped TiO2 photocatalyst and its photodegradation efficiency potential. Mater Chem Phys 220:374–382
30. Kamimura Y, Itabashi K, Okubo T (2012) Seed-assisted, OSDA-free synthesis of MTW-type zeolite and "Green MTW" from sodium aluminosilicate gel systems. Microporous Mesoporous Mater 147(1):149–156
31. Wang B, Dutta PK (2017) Synthesis method for introducing mesoporosity in a faujasitic-like zeolite system from a sodium aluminosilicate gel composition. Microporous Mesoporous Mater 239:195–208
32. Ghrib Y, Frini-Srasra N, Srasra E, Martínez-Triguero J, Corma A (2018) Synthesis of cocrystallized USY/ZSM-5 zeolites from kaolin and its use as fluid catalytic cracking catalysts. Catalysis Sci Technol 8(3):716–725
33. Liu H, Shen T, Wang W, Li T, Yue Y, Bao X (2015) From natural aluminosilicate minerals to zeolites: synthesis of ZSM-5 from rectorites activated via different methods. Appl Clay Sci 115:201–211
34. Jiang J, Duanmu C, Yang Y, Gu X, Chen J (2014) Synthesis and characterization of high siliceous ZSM-5 zeolite from acid-treated palygorskite. Powder Technol 251:9–14
35. Li X-Y, Jiang Y, Liu X-Q, Shi L-Y, Zhang D-Y, Sun L-B (2017) Direct synthesis of zeolites from a natural clay, attapulgite. ACS Sustain Chem Eng 5(7):6124–6130
36. Yu W, Deng L, Yuan P, Liu D, Yuan W, Chen F (2015) Preparation of hierarchically porous diatomite/MFI-type zeolite composites and

their performance for benzene adsorption: the effects of desilication. Chem Eng J 270:450–458
37. Tesson B, Hildebrand M (2010) Dynamics of silica cell wall morphogenesis in the diatom Cyclotella cryptica: substructure formation and the role of microfilaments. J Struct Biol 169(1):62–74. https://doi.org/10.1016/j.jsb.2009.08.013
38. Bäuerlein E (2003) Biomineralization of unicellular organisms: an unusual membrane biochemistry for the production of inorganic nano-and microstructures. Angew Chem Int Ed 42(6):614–641
39. Wang Y, Tang Y, Dong A, Wang X, Ren N, Gao Z (2002) Zeolitization of diatomite to prepare hierarchical porous zeolite materials through a vapor-phase transport process. J Mater Chem 12(6):1812–1818
40. Sanhueza V, Kelm U, Cid R, López-Escobar L (2004) Synthesis of ZSM-5 from diatomite: a case of zeolite synthesis from a natural material. Journal of Chemical Technology & Biotechnology: international Research in process, Environmental & Clean. Technology 79(7):686–690
41. Kordatos K, Gavela S, Ntziouni A, Pistiolas KN, Kyritsi A, Kasselouri-Rigopoulou V (2008) Synthesis of highly siliceous ZSM-5 zeolite using silica from rice husk ash. Microporous Mesoporous Mater 115(1):189–196. https://doi.org/10.1016/j.micromeso.2007.12.032
42. Liu Y, Qiang W, Ji T, Zhang M, Li M, Lu J (2020) Uniform hierarchical MFI nanosheets prepared via anisotropic etching for solution-based sub–100-nm-thick oriented MFI layer fabrication. Sci Adv 6(7):eaay5993
43. Treacy MM, Higgins JB (2007) Collection of simulated XRD powder patterns for zeolites5th edn. Elsevier, Amsterdam
44. Chang A, Yang T-C, Chen M-Y, Hsiao H-M, Yang C-M (2020) Hierarchical zeolites comprising orthogonally stacked bundles of zeolite nanosheets for catalytic and adsorption applications. J Hazard Mater 400:123241. https://doi.org/10.1016/j.jhazmat.2020.123241
45. Vafaeian Y, Haghighi M, Aghamohammadi SJEC, Management (2013) Ultrasound assisted dispersion of different amount of Ni over ZSM-5 used as nanostructured catalyst for hydrogen production via CO2 reforming of methane. Energy Convers Manag 76:1093–1103
46. Busca GJM, Materials M (2017) Acidity and basicity of zeolites: a fundamental approach. Microporous Mesoporous Mater 254:3–16
47. Khanday WA, Majid SA, Shekar SC, Tomar RJMRB (2013) Synthesis and characterization of various zeolites and study of dynamic adsorption of dimethyl methyl phosphate over them. Mater Res Bull 48(11):4679–4686
48. Lónyi F, Valyon JJM, Materials M (2001) On the interpretation of the NH3-TPD patterns of H-ZSM-5 and H-mordenite. Microporous Mesoporous Mater 47(2–3):293–301
49. Tonetto G, Atias J, De Lasa HJACAG (2004) FCC catalysts with different zeolite crystallite sizes: acidity, structural properties and reactivity. Appl Catal A Gen 270(1–2):9–25
50. Al-Dughaither AS, de Lasa HJI, Research EC (2014) HZSM-5 zeolites with different SiO2/Al2O3 ratios. Characterization and NH3 desorption kinetics. Ind Eng Chem Res 53(40):15303–15316
51. Novak S, Chaves TF, Martins L, Santilli CV (2020) Preparation of hydrophobic MFI zeolites containing hierarchical micro-mesopores using seeds functionalized with octyltriethoxysilane. Colloids Surf A Physicochem Eng Asp 585:124109. https://doi.org/10.1016/j.colsurfa.2019.124109